Polymer Chemistry

Accepted Manuscript

ROYAL SOCIETY OF CHEMISTRY

www.rsc.org/polymers

Polymer Chemistry

COMMUNICATION

Glyco-copolypeptide Grafted Magnetic Nanoparticles: The interplay between particle dispersion and RNA loading.

Received 00th January 20xx,
Accepted 00th January 20xx

DOI: 10.1039/x0xx00000x

www.rsc.org/

T. Borase,[a] E. K. Fox,[b] S.-A. Cryan,[c,d,e] D. F. Brougham,[f*] and A. Heise[a,g*]

Lysine-glyco-copolypeptide grafted superparamagnetic iron oxide nanoparticles were prepared through N-carboxyanhydride (NCA) copolymerization. Statistical and block copolymer arrangements were obtained while keeping the overal composition constant. Both type of nanoparticles are fully water dispersable, which is key for T_1-weighted magnetic resonance imaging (MRI) applications. A synergistic effect between siRNA loading and imaging properties was observed in that the statistical copolymer arrangement allowed a significantly higher loading while retaining full particle dispersion, as required for T_1-weighting properties.

Next generation nanomedical materials require the combination of several functions such as imaging and therapeutic delivery, e.g. in theranostics.[1] Materials based on superparamagnetic iron oxide nanoparticles (MNPs) have recently drawn increased interest in that context as MRI agents due to their biocompatibility.[2] While negative contrast (T_2-weighting) is obtained from larger particles or nanoparticle clusters, advantageous positive contrast, arising from localized signal enhancement (T_1-weighting), requires full MNP dispersion and long-term colloidal stability.[3] Colloidal stabilization of MNPs with full particle dispersion can be achieved by surface modification with hydrophilic molecules including polymers.[4] Suitability of superparamagnetic nanoparticles for image-guided gene delivery has been disclosed in a number of reports. For example, Park and co-workers described the use of manganese oxide nanoparticles with electrostatically bound siRNA and demonstrated that this form of delivery can retain siRNA during cellular uptake, when combined with an appropriate targeting method.[5] More recently the Lee group described the use of core@shell $ZnFe_2O_4$@Au NPs manganese oxide nanoparticles with magnetic cellular delivery of electrostatically bound siRNA, with confirmed alterations in gene expression.[6] Zhang synthesised iron oxide NPs coated with chitosan-PEG grafted polyethyleneimine (PEI) shell and conjugated with a monoclonal antibody and demonstrated effective siRNA delivery to cancer cells.[7] It should be noted that in each of these cases significant increases in hydrodynamic size (d_{hyd}) were apparent, probably due to partial aggregation during the loading step. In the case of iron oxide MNPs, this would render the final suspensions suitable for use in T_2-weighted MRI applications only.[3]

We have recently reported a new approach to MNPs with excellent T_1-weighed MRI contrast properties and exceptional colloidal stability by grafting synthetic glycopolypeptides from the MNP surface.[8] Here we report the efficient synthesis of advanced MNPs with combined T_1-weighting and siRNA payload capabilities by co-grafting of two amino acids. In particular, we investigate for the first time how the copolypeptide arrangement influences the loading capacity and the interplay between siRNA loading and imaging properties.

MNPs were functionalized by surface grafting of two amino acid N-carboxyanhydrides (NCA), namely lysine for siRNA polyplex formation[9], and propargyl-L-glutamate (PLG) for glycosylation with galactose by click chemistry.[8,10] The weight composition of the lysine to PLG in the grafted polypeptide was maintained at 4:1 to design polypeptides with high positive charge density, as it was envisaged that relatively fewer sugars would be sufficient to enhance water dispersability. In order to compare the influence of molecular architecture on performance two distinct arrangements were targeted with the same overall copolypeptide composition. In the first instance, a block structure was targeted with poly(L-lysine) (PLL) forming the inner block and the glycosylated poly(propargyl-L-glutamate) (PPLG) the outer block (Scheme 1, left). In a second arrangement both amino acid NCAs were polymerized simultaneously resulting in a statistical

[a] School of Chemical Sciences, Dublin City University, Dublin 9, Ireland.
[b] National Institute for Cellular Biotechnology, Dublin City University, Dublin 9, Ireland.
[c] School of Pharmacy, Royal College of Surgeons in Ireland, Dublin 2, Ireland.
[d] Tissue Engineering Research Group, Royal College of Surgeons in Ireland.
[e] Trinity Centre for Bioengineering, Trinity College Dublin, Dublin 2.
[f] School of Chemistry, University College Dublin, Belfield, Dublin 4, Ireland
[g] Department of Pharmaceutical and Medicinal Chemistry, Royal College of Surgeons in Ireland, Dublin 2, Ireland

Electronic Supplementary Information (ESI) available: FTIR, TGA, DLS, Experimental Procedures. See DOI: 10.1039/x0xx00000x

arrangement of both amino acids on the MNP surface (Scheme 1, right). While the statistical arrangement is synthetically more straightforward, it was anticipated that a block structure would provide distinct compartments for siRNA polyplexes close to the MNPs surface surrounded by a glycosylated periphery.

Scheme 1

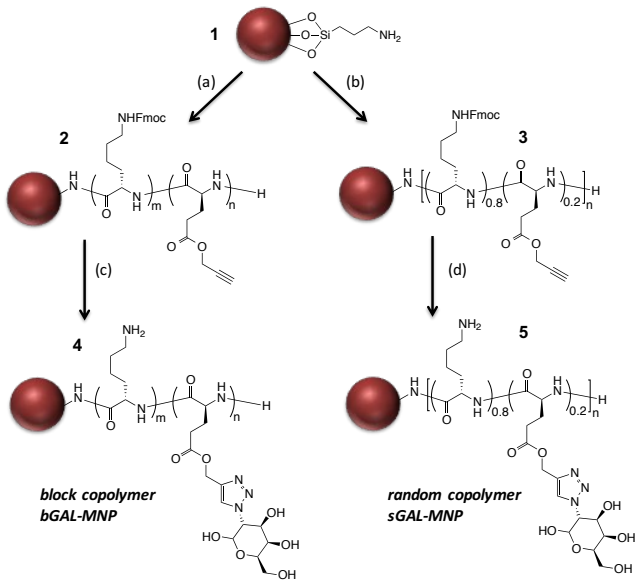

Reagents and conditions: (a) 1. ZLL-NCA, $CHCl_3$, 0°C; 2. PLG-NCA, $CHCl_3$, 0°C; (b) ZLL-NCA, PLG-NCA, $CHCl_3$, r.t.; (c) and (d) 1. $(PPh_3)_3CuBr$, 1-azido-1-deoxy-β-D-galactopyranoside, N-N diisopropylethylamine, anhydrous DMSO; 2. piperidine/DMSO.

Statistical copolymerization was carried out with NCA of fluorenyl-methyl-protected (Fmoc) L-lysine (ZLL) and NCA of PLG (4:1 w/w) from the surface of 8 nm aminopropyl triethoxysilane (APTS) functionalized iron-oxide nanoparticles **1**. ATR-IR analysis of the resulting nanoparticles **3** confirmed the successful grafting of the polypeptides (ESI, Figure S1) evident from the amide I and amide II signals at around 1650 and 1540 cm^{-1}. Moreover, a weak propargyl alkyne band at 2126 cm^{-1} can be identified as well as Fmoc and propargyl ester carbonyl bands around 1705 cm^{-1}. Block copolypeptides PFLL-*b*-PPLG **2** were grafted from the MNPs by sequential addition of the monomers at 0 °C.[11] PFLL was chosen as the first block and after complete monomer conversion, monitored by the absence of anhydride FTIR signals at 1772 and 1880 cm^{-1}, PLG NCA was added. Similar to the statistical copolymers, ATR-IR spectra (ESI, Figure S2) displayed two defined polypeptide amide bands as well as characteristic band of the PLG ester carbonyl (1732 cm^{-1}) and a less intense band for the Fmoc-carbonyl (1690 cm^{-1}). From thermo-gravimetric analysis (TGA) of the statistical copolypeptide grafted MNP **3**, an organic content of 80% was calculated. For the block grafted MNPs following the first PZLL block an organic weight loss of 67% between 150 to 650°C was recorded. After polymerization of the second block this increased to 80% for **2** (ESI, Figures S3 and S4). These observations are consistent with the targeted block length ratio of 4:1.

The PLG of both statistical and block copolypeptide decorated MNPs were glycosylated with azido galactose using copper catalyzed Huisgen's click chemistry.[8] In a subsequent step, Fmoc was removed from ZLL by addition of pipyridine to the MNP suspension in DMF. The final products MNP-(PLL-*st*-(PPLG-Gal)) **5** and MNP-(PLL-*b*-(PPLG-c-Gal)) **4** were then recovered as dry products by lyophilization, we will refer to these as *s*GAL-MNP and *b*GAL-MNP, respectively. TGA analysis (ESI, Figure S3) of the final product *b*GAL-MNP revealed an organic content of 70%. This overall decrease in organic content (~ 10%) after glycosylation (theoretical addition of 40 wt%) and Fmoc deprotection (theoretical removal of 52 wt%) is in agreement with quantitative glycosylation and deprotection at a comonomer ratio of 4:1. Similar quantitative results were obtained from the TGA analysis of the *s*GAL-MNP samples (ESI, Figure S4).

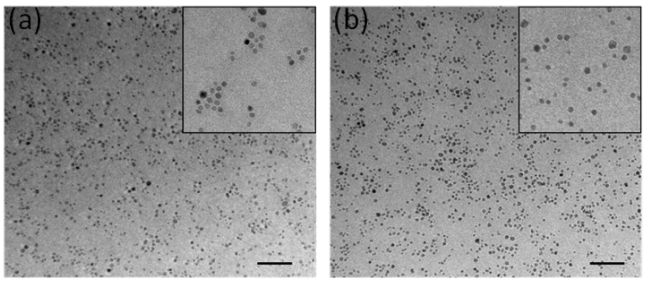

Figure 1. Representative transmission electron microscopy (TEM) images of (a) *sGAL*-MNP **5** and (b) *b*GAL-MNP **4** grafted iron oxide nanoparticles. The scale bar is 100 nm. The inset shows zoomed images (x2) of well-dispersed nanoparticles.

Transmission electron microscopy (TEM) analysis of dried samples confirmed the presence of individual particles (Figure 1). The diameter (d_{core}) of both *s*GAL-MNPs and *b*GAL-MNPs was determined from the micrographs to be 8.2±2.0 nm, which is very similar to that of the underivatised NPs (Figure S9, ESI). Both types of glycopolypeptide grafted MNPs displayed excellent water dispersability. Dynamic light scattering (DLS) confirmed the suspensions are formed from fully dispersed individual particles, which is a key requirement for T_1-weighting in MRI,[12] with typical d_{hyd} values of ≤18 nm measured (ESI, Figure S5). The d_{hyd} values are greater than d_{core}, as expected, due to the polypeptide shell, particle hydration and statistical weighting of the DLS response to larger particles in the distribution. Critically, very low polydispersity indices, PDI values, were measured for the glycopeptide grafted MNP suspensions in particular, with values of c.0.08-0.12, Table 1, unchanged over a period of at least 26 weeks. Moreover, ζ potential measurements on the suspensions confirm the presence of positively charged particles (Table 1). The ζ value is slightly reduced, as expected, for the glycosylated MNP suspensions, and in particular for the block copolypeptide MNP as in this case the lysine is predominantly closer to the core.

Table 1. Physical properties of aqueous MNP dispersions.

Sample	d_{hyd} (PDI) [nm]	ζ [mV]	Relaxivity (61 MHz) r_1, r_2 (r_2/r_1) [$s^{-1}mM^{-1}$, $s^{-1}mM^{-1}$,-]
PLL-MNP	18.5(0.18)	+56	17.9, 80.9 (4.5)
sGAL-MNP, **5**	14.9(0.12)	+47	16.2, 70.5 (4.4)
*b*GAL-MNP, **4**	18.5(0.09)	+31	16.9, 78.1 (4.6)

The efficacy of an MNP suspension for generating contrast by enhancing local MRI signal is measured by the spin–lattice (r_1) and spin-spin (r_2) relaxivities, respectively. These are the water relaxation enhancements per millimolar concentration of Fe. Hence we studied the relaxivity of PLL-MNP, *s*GAL-MNP and *b*GAL-MNP suspensions using conventional and fast field-cycling NMR relaxometry (NMRD). The latter technique involves the measurement of r_1 as function of field strength and hence ^{1}H Larmor frequency (Figure 2 and Table 1 and ESI, Table S2).

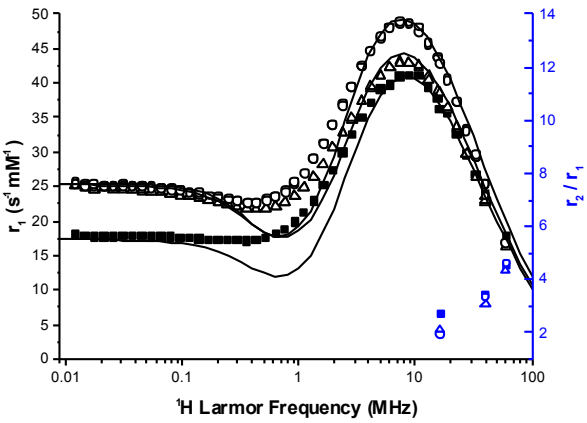

Figure 2. ^{1}H NMRD profiles and relaxivity ratios, at 298 K, for aqueous PLL-MNP (■), sGAL-MNP (Δ) and bGAL-MNP (○) suspensions. The solid line are simulations using SPM theory, see text.

The key points are the high r_1 values, c.16-17 $s^{-1}mM^{-1}$, and low r_2/r_1 ratios of c.4.5, in the clinical MRI range (61 MHz). These values are comparable to those identified for other T_1-agents,[4,8] but with the addition of the functional polymer for the first time. The characteristic shape of the ^{1}H profiles confirms superparamagnetic behaviour of the particles in suspension.[13] Firstly, the frequency of the maximum, ν_{max}, which is known to be very sensitive to the size of the inorganic core, is constant (c.8 MHz) for all three suspensions, suggesting full particle dispersion. Note the same bare NPs were used to prepare the three suspensions. Secondly, an r_1 minimum in the 0.1-1 MHz range is observed for the glycosylated MNPs only; this is characteristic of small fully dispersed particles[4,8] which therefore have very low magnetocrystalline anisotropy, ΔE_{anis}.[4,13] Its absence for the PLL-MNPs suspension is consistent with some minor aggregation for that sample, an effect that does not show up in the r_2 and r_2/r_1 or d_{hyd} values (Table 1). Interestingly, this sample exhibits a higher PDI, of 0.18, although it is stable to further aggregation in water for weeks. It is clear that the PDI value and the presence of a low MHz range minimum are the most sensitive measures of particle dispersion for these samples. The differences in relaxivity when the stabilising polymer is changed from *s*GAL-MNP **5** to *b*GAL-MNP **4** for the MRI application are minor. The superparamagnetic response can be simulated[13] (Figure 2 and Table S1). Note that the mid-frequency discrepancy between experiment and theory arises because of the latter involves an interpolation between the high- and low-frequency relaxation mechanisms. However this difference is not important as the parameters extracted from the simulation are not sensitive to r_1 values in this range.[13] This approach suggests a slight, c.4%, relative increase in the magnetization sensed by the diffusing H_2O molecules in the case of the *b*GAL-MNPs, see ESI. We believe that this enhancement arises from the polymer architecture, it is subject of ongoing studies.

The presence of galactose was further demonstrated by binding experiments with galactose selective Ricinuscommunis Agglutinin (RCA_{120}) lectin. With the addition of the lectin rapid aggregation of the MNPs through selective multivalent binding was observed with the resulting aggregates capable of being trapped in a moderate external magnetic field gradient (Figure 3).

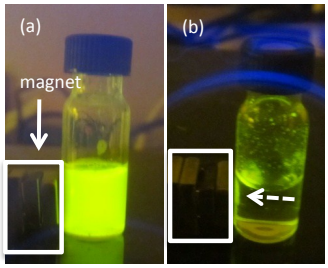

Figure 3. Photographic images showing selective binding of fluorescently tagged *b*GAL-MNP **4** to lectin RCA_{120}. (a) FITC tagged nanoparticle dispersion in PBS buffer solution. (b) Magnetically captured nanoparticle aggregates (broken arrow) after addition of RCA_{120}.

Small interfering RNA (siRNA) was used to demonstrate the ability of the MNPs to encapsulate nucleic acids by electrostatic binding arising from the the positively charged lysine units. GAL-MNP suspensions containing increasing concentrations of MNP's in deionized water were mixed with a fixed amount of siRNA and allowed to complex for 30 min. at room temperature. Gel retardation assays (Figure S8, ESI) confirm a maximum loading at siRNA/*b*Gal-MNP ratio of 38.3 nmol/mg. While this experiment provides information about the absolute loading capacity of Gal-MNP with siRNA it does not provide any information on whether the loading results in nanoparticle aggregation. In order to maintain T_1-weighed MR properties, the maximum siRNA loading possible while maintaining full polyplex dispersion is the key issue. This value was determined by sequential addition of aliquots of siRNA to a known volume of MNP suspension. The suspensions were monitored by DLS with a view to maintaining colloidal stability, with PDI ≤0.20, *i.e.* while adhering to our previously established criterion for full dispersion. It was found that *s*GAL-MNP suspensions showed 2.2 nmol/mg siRNA loading (c. 1.6 siRNA chains per MNP) with PDI <0.20 (Figures S10 and S11, ESI). For *b*GAL-MNP suspensions it was only possible to reach

0.3 nmol/mg while adhering to the same criterion. Our interpretation is that, given the similar organic content, monomer ratios and quantitative glycosylation, lower loading arises due to the block copolymer architecture. For *s*GAL-MNP suspensions the PLL component is more accessible and more siRNA can be accommodated in the outer part of the polymer shell without excessive chain disruption, resulting in better colloidal stability at higher siRNA content.

In conclusion, we have reported fully dispersed superparamagnetic iron oxide NPs useful for T_1-weighed MRI, which are also capable of carrying siRNA payloads without loss of colloidal stability. At a constant overall composition, it was found that the structural variation of the copolymer did not significantly influence the imaging properties. However, there was a distinct synergistic influence in that the statistical polypeptide arrangement allowed higher siRNA loading without compromising the particle dispersion. This work highlights the need for careful material engineering on the nanoscale to meet the demanding requirements of nanomaterials combining multiple functions. Further work will focus on the biocompatibility and *in vitro* studies.

Financial support from the Science Foundation Ireland (SFI) Principle Investigator Awards 07/IN1/B1792 and 13/IA/1840 is gratefully acknowledged. EF acknowledges financial support from the European Union's Seventh Framework Programme for research, technological development and demonstration under grant agreement N° 310250 (project UNION).

Notes and references

1 (a) J. Funkhouser, *Curr. Drug Disc.* 2002, **2,** 17. (b) H. J. Ryu, H. Koo, I. Sun, S. H. Yuk, K. Choi, K. Kim and I. C. Kwon, *Adv. Drug Deliv. Rev.* 2012, **64**, 1447. (c) M. S. Shim and Y.J. Kwon, *Adv. Drug Deliv. Rev.* 2012, **64**, 1046. (d) H. Koo, M. S. Huh, I. Sun, S. H. Yuk, K. Choi, K. Kim and I. C. Kwon, *Acc. of Chem. Res.* 2011, **44**, 1018.

2 (a) C. Corot and D. Warlin, *Wiley Interdisc. Rev. Nanomed. Nanobiotechnol.* 2013, **5**, 411. (b) J. Gallo, N. Kamaly, I. Lavdas, E. Stevens, Q.-D. Nguyen, M. Wylezinska-Arridge, E. O. Aboagye and N. J. Long, *Angew. Chem. Int. Ed.* 2014, **53**, 9550.

3 U. I. Tromsdorf, O. T. Bruns, S. C. Salmen, U. Beisiegel and H. Weller, *Nano Lett.* 2009, **9**, 4434.

4 T. Ninjbadgar and D. F. Brougham, *Adv. Funct. Mater*. 2011, **21**, 4769.

5 K. H. Bae, K. Lee, C. Kim and T. G. Park, *Biomaterials* 2011, **232**, 176.

6 B. Shah, P. T. Yin, S. Ghoshal and K.-B Lee, *Angew. Chem. Int. Ed.* 2013, **52**, 6190.

7 K. Wang, F. M. Kievit, J. G. Sham, M. Jeon, Z. R. Stephen, A. Bakthavatsalam, J. O. Park and M. Zhang, *Small* 2016, **12**, 477.

8 T. Borase, T. Ninjbadgar, A. Kapetanakis, S. Roche, R. O'Connor, C. Kersken, A. Heise and D. F. Brougham, *Angew. Chem. Int. Ed.* 2013, **52**, 3164.

9 (a) K. Itakaa, K. Yamauchia, A. Haradaa, K. Nakamurab, H. Kawaguchib and K. Kataoka, *Biomaterials* 2003, **24**, 4495. (b) D. W. Pack, A. S. Hoffman, S. Pun and P. S. Stayton, *Nature Rev. Drug Discov.* 2005, **4**, 581. (c) Z. Kadlecova, Y. Rajendra, M. Matasci, L. Baldi, D. L. Hacker, F. M. Wurm and H.-A. Klok, J. *Control. Release* 2013, **169**, 276. (d) M. Byrne, D. Victory, A. Hibbitts, M. Lanigan, A. Heise and S-A. Cryan, *Biomater. Sci.* 2013, **1**, 1223.

10 (a) K. Ren, C. He, C. Xiao, G. Li and X. Chen, *Biomaterials* 2015, **51**, 238. (b) A. C. Engler, H. Lee and P. T. Hammond, *Angew. Chem. Int. Ed.* 2009, **48**, 9334.

11 T. Borase, M. Iacono, S. I. Ali, P. D. Thornton and A. Heise, *Polym. Chem.* 2012, **3**, 1267.

12 C. J. Meledandri and D. F. Brougham, *Anal. Methods* 2012, **4**, 331.

13 A. Roch, R. N. Muller and P. Gillis, *J. Chem. Phys.* 1999, **110**, 5403.

Table of Content Artwork